Eur J Nucl Med Mol Imaging (2016) 43:953–963
DOI 10.1007/s00259-015-3218-z

ORIGINAL ARTICLE

In vivo biokinetic and metabolic characterization of the ^{68}Ga-labelled α5β1-selective peptidomimetic FR366

Calogero D'Alessandria[1] · Karolin Pohle[1] · Florian Rechenmacher[2] · Stefanie Neubauer[2] · Johannes Notni[3] · Hans-Jürgen Wester[3] · Markus Schwaiger[1] · Horst Kessler[2] · Ambros J. Beer[1,4]

Received: 18 June 2015 / Accepted: 6 October 2015 / Published online: 24 October 2015

Abstract
Purpose Integrins are transmembrane receptors responsible for cell–cell adhesion and cell–extracellular matrix binding and play an important role in angiogenesis and tumour metastasis. For this reason, integrins are increasingly used as targets for molecular imaging. Up to now interest has mostly been focused on the integrin subtype αvβ3. However, targeting of other subtypes such as the integrin α5β1 is also of high interest due to its central role in colonization of metastatic cells, resistance of tumour cells to chemotherapy and ionizing radiation, and tumour aggressiveness. Recently, a highly active antagonist ligand (2,2′-(7-(1-carboxy-4-((6-((3-(4-(((*S*)-1-carboxy-2-(2-(3-guanidinobenzamido)acetamido)ethyl)carbamoyl)-3,5-dimethylphenoxy)propyl)amino)-6-oxohexyl)amino)-4-oxobutyl)-1,4,7-triazonane-1,4-diyl)diacetic acid, FR366) for the integrin subtype α5β1 with high selectivity versus αvβ3, has been developed and tested successfully in preliminary in vitro and in vivo experiments. Here, we present our results of an investigation of the use of ^{68}Ga-labelled α5β1 ligand in PET imaging.
Methods The free α5β1 peptidomimetic ligand was functionalized with a spacer (6-aminohexanoic acid) and the bifunctional chelator 1-((1,3-dicarboxy)propyl)-4,7-(carboxymethyl)-1,4,7-triazacyclononane (NODAGA) to yield FR366 and labelled with ^{68}Ga. To confirm selective in vivo targeting of α5β1, female BALB/c nude mice xenografted with α5β1-expressing RKO cells in the right shoulder and α5β1/αvβ3-expressing M21 cells in the left shoulder were subjected to PET/CT scans and biodistribution experiments. Specificity of tracer uptake was proven by blocking studies. Metabolic stability of the injected tracer was measured in urine and in plasma.
Results MicroPET/CT scans with radiolabelled FR366 showed a good tumour-to-normal tissue ratio with low uptake in the liver (0.32±0.14 %ID/g) and good retention of ^{68}Ga-NODAGA-FR366 in the tumour (0.71±0.20 %ID/g and 0.40 ±0.12 %ID/g for RKO and M21 tumours, respectively, at 90 min after injection). Biodistribution experiments showed uptake in the α5β1-expressing RKO tumour of 1.05± 0.23 %ID/g at 90 min after injection. Specificity of tracer uptake was demonstrated by injection of 5 mg/kg unlabelled ligand 10 min prior to tracer injection, resulting in a 67 % reduction in uptake in the RKO tumour. The tracer was found to be metabolically stable in urine and plasma 30 min after injection.
Conclusion Our results show that PET imaging of α5β1 expression with the ^{68}Ga-labelled α5β1-specific ligand is feasible with good image quality. Thus, FR366 is a promising new tool for investigating the role of α5β1 in angiogenesis and the

Calogero D'Alessandria and Karolin Pohle contributed equally to this work.

✉ Calogero D'Alessandria
calogero.dalessandria@tum.de

[1] Nuklearmedizinische Klinik und Poliklinik, Klinikum rechts der Isar, Technische Universität München, Ismaninger Str. 22, 81675 München, Germany

[2] Institute for Advanced Study (IAS) and Center of Integrated Protein Science (CIPSM), Department Chemie, Technische Universität München, Lichtenbergstrasse 4, 85747 Garching, Germany

[3] Lehrstuhl für Pharmazeutische Radiochemie, Technische Universität München, Walther-Meißner-Str. 3, 85748 Garching, Germany

[4] Present address: Department of Nuclear Medicine, Ulm University, Albert-Einstein-Allee 23, 89081 Ulm, Germany

influence of this integrin subtype on cancer aggressiveness and metastatic potential.

Keywords α5β1 · Integrin antagonist · Peptidomimetics · PET imaging

Introduction

Integrins are a family of adhesion molecules responsible for cell binding to extracellular matrix (ECM) proteins. They consist of 24 αβ heterodimers that play fundamental roles in cell growth, the cell cycle, differentiation, apoptosis, survival and motility, angiogenesis and tumour metastasis [1]. The ECM provides both structural support and extracellular cues that regulate invasive tumour growth, and tumour-associated changes in ECM contribute to cancer progression. Integrins are important in tumour development, tumour angiogenesis and metastasis [2]. They hold a critical position as transducers of chemical and mechanical signals that control tumour cell responses to ECM binding (i.e. outside-inside signalling), as well as tumour-mediated changes to the ECM that facilitate invasive growth and metastasis (i.e. inside-outside signalling) [3, 4]. Many members of the integrin family, including α5β1, α8β1, αIIbβ3, αvβ3, αvβ5, αvβ6 and αvβ8, recognize an Arg-Gly-Asp (RGD) motif within their ECM ligands such as collagen, laminin, fibronectin, vitronectin and other large glycoproteins [4].

Based on these findings, monomeric and multimeric linear as well as cyclic peptides including the RGD motif have been developed for therapeutic approaches or for molecular imaging of integrin expression [5–8]. Up to now, most work in this field has been done on the integrin subtype αvβ3. The first example of using a peptide for αvβ3 imaging was the pentapeptide cyclo(-Arg-Gly-Asp-DPhe-Val-) developed by us, which shows high affinity for αvβ3 and selectivity against αIIbβ3 [9]. The drug candidate cilengitide, the N-methylated (at valine) derivative of this cyclic peptide, has shown strong attenuation activity on tumour angiogenesis and tumour growth in many preclinical studies and is currently in clinical phase II for the treatment of several tumour types [10, 11].

By conjugating the cyclic pentapeptide to glucose-based or galactose-based sugar amino acids, several tracers for SPECT and PET imaging have been developed [12–14]. Preclinical imaging studies have shown the selectivity and specificity of these tracers [14, 15]. Moreover, the correlation between αvβ3 expression and tracer accumulation has also been demonstrated [16]. [^{18}F]Galacto-RGD was the first PET tracer used in patients for targeting the αvβ3 integrin with good image quality [17]. Preoperative quantification of αvβ3 expression uptake in tumour lesions using [^{18}F]galacto-RGD PET showed significant correlation with the αvβ3 expression determined by immunohistochemical staining of surgical specimens [18]. However, in recent years it has become increasingly clear that the role of the integrin αvβ3 is complex, which often complicates the interpretation of imaging data with respect to their biological meaning and clinical significance [19, 20].

Concerning other integrin subtypes, upregulated expression of α5β1 has also been reported in tumour vasculature and other cancer cells [21]. The integrin subunit β1 has been shown to play a key role in reorganizing and changing the cytoskeletal architecture of dormant cells to metastatic cells in vitro and in vivo and in the extravasation and colonization of metastatic cells [22, 23]. Integrin β1 is responsible for resistance of tumour cells to chemotherapy and ionizing radiation in vitro and in mice bearing xenografts [24]. Clinical studies have provided evidence that high expression of α5β1 is associated with a more aggressive phenotype in brain tumours, in particular high α5 gene expression is associated with decreased survival of patients with high-grade glioma [25].

Thus, the design and synthesis of antagonists that specifically inhibit the integrin RGD-containing binding site is of high interest not only for the development of selective drugs for therapy but also for selective molecular imaging of this integrin subtype. Recently, we have designed nonpeptidic RGD-based integrin antagonists that specifically target (and block) α5β1 and αvβ3 while maintaining selectivity against the platelet integrin αIIbβ3 and have demonstrated the first selective imaging for these two integrins in a proof of principle study [26–28]. We present here a complete in vivo characterization of the ^{68}Ga-labelled α5β1-selective antagonist FR366 to specifically monitor α5β1 integrin expression in vivo.

Materials and methods

Materials

The α5β1 integrin antagonist was synthesized and functionalized with the chelator NODAGA as previously reported [26, 28]. HCl (1.0 M) for elution of the ^{68}Ge/^{68}Ga generator was prepared from HCl (Suprapur®) and water (Ultrapur®), both obtained from Merck. Ultrapur water was also used for all radiochemical work, including the preparation of precursors and buffer solutions. 2-[4-(2-Hydroxyethyl)-1-piperazinyl]-ethanesulphonic acid (HEPES) was obtained from Merck. Radio-TLC was performed on Varian glass microfibre chromatography papers impregnated with silicic acid (#A120B12). Readout of chromatograms was done using a Bioscan TLC scanner, consisting of a B-MS-1000 scanner, a B-EC-1000 detector with a B-FC-3600 GM tube.

Peptide labelling with ^{68}Ga

The method used for ^{68}Ga labelling was similar to previously published procedures on a fully automated system (GallElut^{+} from Scintomics GmbH, Fürstenfeldbruck, Germany) [29]. For elution of the ^{68}Ge/^{68}Ga generator with SnO_2 matrix (iThemba LABS, Faure, South Africa) 1.0 M aqueous HCl was used. The generator was preeluted 2 – 4 h prior to production with 10 mL HCl in order to minimize the content of metal ion contaminants. For production, an eluate fraction of 1.25 mL containing approximately 80 % of the entire activity (about 1.0 GBq) was transferred into a standard reactor vial (Alltech, 5 mL) containing the precursor (1 or 2 nmol) and an aqueous solution of HEPES (600 mg HEPES in 500 μL water; resulting pH 3.3). The vial was heated to 95 °C for 5 min while air was slowly bubbled though the solution for agitation. The mixture was then passed through a SPE cartridge (Waters SepPak® C18 classic) that had previously been conditioned by purging with ethanol (5 mL, absolute, Ph. Eur.) and water (10 mL). The cartridge was then purged with water (10 mL) and air (10 mL). The labelled product was eluted from the cartridge into a 10-mL flask with 1 mL ethanol, followed by purging with phosphate-buffered saline (PBS; 1 mL, pH 7.4) and water (1 mL). The product was concentrated in vacuum to 1 mL, such that no ethanol was left in the mixture and the solution exhibited the appropriate pH and osmolality for injection. Before injection, the formulation was filtered through a sterile filter (0.22 μm).

Radio-TLC of the radiolabelled product was performed using two different eluents: TLC-A comprised 0.1 M aqueous sodium citrate as mobile phase, free $^{68}Ga^{3+}$ is eluted with the solvent front (R_F about 0.8 – 1) as citrate complex, and the product stays at the origin (R_F=0.1); TLC-B comprised 1.0 M NH_4OAc/MeOH (1:1) as mobile phase, insoluble colloidal $^{68}Ga^{III}$ stays at the origin (R_F=0) and the radiolabelled product is eluted (R_F=0.5 – 0.6). Radio-HPLC was performed on a Sykam system using a Chromolith column (Merck, 100× 4.6 mm), flow rate 2.0 mL/min, with radioactivity and UV detection (220 nm). Eluents were water (A) and acetonitrile (B), both containing 0.1 % trifluoroacetic acid (isocratic elution with 3 % B for 2 min, followed by a gradient to 60 % B in 6 min and isocratic elution with 95 % B for 3 min). The retention time of the ^{68}Ga-labelled product was 6.1 min. Radiochemical purity was >95.0 % as determined by radio-TLC and >98.0 % using radio-HPLC.

Partition coefficient

Approximately 0.5 MBq of the radiolabelled ligand in 500 μL PBS was added to 500 μL octanol in an Eppendorf tube. After vigorous mixing for 3 min at room temperature the vials were centrifuged at 15,000 *g* for 1 min, and 100-μL aliquots of both layers were counted in a gamma counter. The experiment was repeated six times.

Cell lines and animal tumour models

Human M21 melanoma cells and human RKO colon carcinoma cells (ATCC® CRL-2577™) were selected for this study based on their different integrin expression pattern (α5β1 versus αvβ3). M21 cells were cultivated in RPMI 1640 medium supplemented with 10 % fetal bovine serum (FBS) and 1 % gentamicin (all from Biochrom AG, Berlin, Germany), and RKO cells were cultivated in Earle's MEM supplemented with 10 % FBS and 1 % L-glutamine (Biochrom) at 37 °C in a humidified atmosphere containing 5 % CO_2. The tumour xenograft models were generated by subcutaneous injection of the cells suspended in PBS (Biochrom) into the shoulder of female BALB/c nude mice (Charles River, Germany) at 6 – 8 weeks of age. M21 cells (1.0×10^7) and RKO cells (1.0×10^7) were injected into the left and right shoulder, respectively. Two weeks after inoculation the mice were subjected to dynamic microPET/CT and biodistribution studies (tumour volume approximately 200 – 500 mm^3). All animal experiments were performed in accordance with current animal welfare regulations in Germany.

Flow cytometry analysis

M21 and RKO cells were both investigated for expression of αvβ3 and α5β1. In brief, M21 and RKO cells at 80 % confluence were harvested using Accutase® (Gibco®, Life Technologies) and washed with HEPES buffer (20 mM HEPES, 125 mM NaCl, 45 mM glucose, 5 mM KCl, 0.1 % albumin, 1 mM $MnCl_2$, pH 7.4). Cells were incubated at a concentration of 1×10^6 cells/25 μL of HEPES-buffer with mouse antibodies against human integrin αvβ3 (FITC-labelled, MAB1976F, dilution 1:12; Millipore) or α5 (10 F6, ab93943, dilution 1:3; Abcam). Isotope-matched FITC-conjugated antibodies were used as controls. After 30 min incubation at 4 °C, cells were washed twice with cold HEPES buffer. For αvβ3 analysis, cells were suspended in 400 μL buffer. For α5β1, cells were incubated with goat antimouse IgG H&L FITC-labelled secondary antibody (ab7064; Abcam) for 30 min, washed twice and suspended in 400 μL buffer. Flow cytometry was performed using a FACSCanto II system (Becton Dickinson, Heidelberg, Germany). Data were analysed using FlowJo 8.8.6 software.

Internalization assay

In vitro integrin binding studies were performed on M21 and RKO cells. To determine nonspecific binding, incubation with 4 μmol/L cilengitide was included. Cells were incubated for 5, 15, 30, 45, 60 and 120 min at 37 °C. One day prior to the

experiment, the cells were harvested using trypsin/EDTA (0.05 % and 0.02 %) in PBS (Biochrom), centrifuged and resuspended in culture medium. The cells were transferred into 24-well plates (approximately 200,000 cells per well in 1 mL) and placed in the incubator overnight. The plates were used when confluence had reached approximately 80 %. The culture medium was removed 30 min before the start of the experiment and binding buffer, comprising 25 mmol/L Tris(hydroxymethyl)aminomethane (Tris) pH 7.4, 150 mmol/L NaCl and 1 mmol/L $MnCl_2 \cdot 4H_2O$ at 0.1 % (m/m) in BSA, was added. The cells were incubated with the ^{68}Ga-labelled ligand (300,000 cpm/well) diluted in binding buffer. The total incubation volume was 250 μL. After incubation the supernatant (unbound tracer) was collected, the cells were washed with cold binding buffer and incubated twice with cold acid wash buffer (50 mM sodium acetate in 0.9 % NaCl, pH 4.5). The supernatant was collected (membrane-bound tracer) and the cells were removed from the plate with 1 M sodium hydroxide solution and transferred to vials for determination of internalized tracer. The radioactivity of all solutions was measured in a gamma counter. The experiments were performed in triplicate. The results were corrected for nonspecific binding and are presented as the total bound activity (membrane-bound and internalized activity).

Biodistribution studies

Biodistribution studies were performed in female BALB/c nude mice at 6 – 8 weeks of age bearing RKO (right shoulder) and M21 (left shoulder) tumour xenografts. Mice were anaesthetized with isoflurane and 5 – 10 MBq of ^{68}Ga-NODAGA-α5β1 ligand (35.8 ng per animal) was injected via a tail vein. Blocking experiments were performed by injection of 100 μg (approximately 5 mg/kg body weight) of the unlabelled precursor 10 min before tracer injection. Mice were killed directly after PET scanning (90-min dynamic scans). Blood, tumours, organs and tissue were excised, collected and wet-weighed. The radioactivity was measured using a gamma counter (1480 Wizard; PerkinElmer Wallac). The results are presented as percentage of injected dose per gram of tissue (%ID/g) and values are expressed as means±SD. A group of ten animals was used for the investigation of ^{68}Ga-NODAGA-FR366 ligand, and a group of five for the blocking experiments.

MicroPET imaging

PET imaging was performed using a Siemens Inveon small-animal PET/CT scanner (Siemens, Knoxville, TN). The animals were anaesthetized with isoflurane and 10 – 14 MBq of radiotracer was injected via a tail vein. For blocking experiments, 100 μg of unlabelled precursor in 50 μL PBS was injected 10 min prior to tracer administration. Static scans were acquired 75 min after injection for 15 min, and 90-min dynamic scans were started together with tracer injection (46 frames: 6×5 s, 21×10 s, 8×2 min, 8×5 min, 3×10 min). Inveon Research Workplace was used for data analysis. The images were reconstructed using a three-dimensional ordered-subsets expectation maximization (OSEM3D) algorithm without scatter and attenuation correction. For time–activity curve analysis, the volumes of interest were defined on dynamic scans using the sum of the last two frames of the image dataset (70 – 90 min).

In vivo stability

Metabolic stability was evaluated in the same mouse model as described above. Radiolabelled ligand (30 – 40 MBq) was injected via a tail vein under isoflurane anaesthesia. After 30 min, the animals were killed and samples were taken from blood, urine, liver, kidneys, and tumour. Urine was ultrafiltered (Amicon Ultra-0.5 mL centrifugal filters, 30 kDa molecular weight cut-off, Ultracel regenerated cellulose, Millipore; Merck KGaA, Darmstadt, Germany). Blood was immediately centrifuged for 5 min at 11,500 *g*, the plasma separated from the pellet, and both components measured in a gamma counter for determination of blood cell bound activity. The plasma was then ultrafiltered. Organs were frozen in liquid nitrogen and homogenized using a Mikro Dismembrator II ball mill (B. Braun, Melsungen, Germany). The homogenate was suspended in PBS (pH 7.4, 200 – 500 μL), shaken vigorously for 1 min, and centrifuged for 5 min at 11,500 *g*. After removal of supernatants, the pellets were washed with 200 – 400 μL PBS and centrifuged again. Supernatants of both centrifugation steps were combined. To determine extraction efficiency, the radioactivity of the supernatant and the pellet was measured in a gamma counter. The supernatant was ultracentrifuged at 11,500 *g* for 10 min using Amicon Ultra centrifugal filters. Samples of the filtrate were analysed by radio-TLC (Merck PLC glass plates 20 × 20 cm, silica gel 60 F_{254} 2 mm with concentration zone; Merck KGaA, Darmstadt, Germany) with MeOH/1 M NH_4OAc 1:1 as the mobile phase. Autoradiography of the chromatograms was performed using Fujifilm imaging plates (BAS-IP MS2025) and a computer radiography reader (CR 35 Bio; Dürr Medical). Data were analysed using AIDA image analyser 4.24 software.

Results

^{68}Ga-labelling

Radiolabelling was performed using a fully automated production process. A fraction of the generator eluate was adjusted to pH 3.3 with HEPES and labelling was performed for 5 min at 95 °C. A precursor amount of 1 or 2 nmol was

sufficient to obtain good radiochemical yield and high specific activity of the product, similar to previous results with ^{68}Ga-NODAGA-c(RGDyK) [29]. Starting with 1.0 GBq of total initial activity, ^{68}Ga-labelling yield was 80.5±11.0 % and 83.81±4.13 % using, respectively, 1 or 2 nmol of the precursor, resulting in a specific activity of 684±91 or 356±18 GBq/μmol at the end of synthesis. For other ligands with the NODAGA chelator, the labelling efficiency is significantly influenced by the quality of the generator eluate when these low precursor amounts are employed. Therefore, the generator was routinely pre-eluted 2 – 4 h before synthesis to ensure similar conditions for each labelling.

The octanol–water partition coefficient (log*P*) was −3.91± 0.09 for the ^{68}Ga-NODAGA-FR366 antagonist. According to in vivo studies, the high hydrophilicity causes significant kidney excretion and moderate accumulation in the liver and adrenal glands (see biodistribution analysis).

Flow cytometry analysis and internalization assay

To investigate in vitro cell binding of the ^{68}Ga-NODAGA-FR366 antagonist, cell surface integrin expression was determined in RKO human colon carcinoma cells and in M21 human melanoma cells. FACS analysis verified high α5β1 expression on the RKO cell membrane and lower expression on the M21 cell membrane (Fig. 1a). Cells of both cell lines bound the α5β1 antibody and the resulting signal could be clearly differentiated from the isotype control. The mean fluorescence intensity was higher for RKO cells than for M21 cells (relative fluorescence intensity 73.7 vs. 53.8), indicating a higher density of α5β1 on the RKO cell surface. Interestingly, a lack of αVβ3 expression on the RKO cell membrane was demonstrated by FACS analysis in contrast to the high αVβ3 expression on the M21 cell membrane (relative fluorescence intensity 8.3 vs. 50.3; Fig. 1b).

The internalization assay (Fig. 2) showed fast early accumulation of the radiotracer in M21 melanoma cells corresponding to 10.4 % of the activity added (300,000 cpm/well) internalized after 30 min incubation followed by slow release in the remaining 90 min of the test. After 120 min the amount of internalized activity reached 8 %. In contrast, slow accumulation of the radiotracer was seen in RKO cells. After 30 min incubation the amount of internalized activity reached 8 % of the activity added (300,000 cpm/well) with a slow increase in internalization during the remaining 90 min of incubation. After 120 min 9.2 % of the added activity was bound to or internalized in the cells. All data were corrected for ^{68}Ga decay.

Biodistribution studies

Biodistribution studies were performed in female BALB/c nude mice at 6 – 8 weeks of age bearing RKO (right shoulder) and M21 (left shoulder) tumour xenografts. Blocking experiments were performed by injection of 100 μg (approximately 5 mg/kg body weight) of the unlabelled precursor (NODAGA-coupled α5β1 antagonist) 10 min before tracer injection. The mice were injected with 5 – 10 MBq of the radiotracer (mean±SD 31.6±4.3 ng per animal) with a specific activity of 243.8±29.9 GBq/μmol (mean±SD) at the time of injection. Tracer uptake values in RKO and M21 tumours were 1.05±0.23 and 0.64±0.26 %ID/g, respectively (Fig. 3). The calculated RKO tumour-to-blood ratio was 15.50) and RKO tumour-to-muscle ratio was 28.06, suggesting that in-vivo visualization of the tumours with good contrast should be feasible (Table 1). Owing to the high hydrophilicity of the tracer, low to moderate uptake was seen in the liver and intestines (0.32±0.14 %ID/g in the liver, 0.20±0.12 %ID/g in the small intestine, 0.31±0.07 %ID/g in the large intestine) and high uptake in the kidneys (1.24±0.22 %ID/g). The specificity of the tracer was proven by efficient blocking of uptake in both RKO and M21 tumours (0.34±0.15 %ID/g and 0.29± 0.07 %ID/g, respectively), resulting in a reduction in tracer uptake of 67 % and 54 %, respectively.

MicroPET imaging

The in vivo targeting ability of the α5β1-selective compound was evaluated by microPET/CT imaging. The ^{68}Ga-labelled tracer showed higher uptake in RKO tumours than in M21 tumours (Fig. 4a–c). In static scans of four mice, the median uptake values in regions of interest drawn around the tumours were 0.71±0.20 %ID/g for the RKO tumours and 0.40±0.12 %ID/g for the M21 tumours (mean±SD). The tumours were clearly distinguishable from nontarget tissues as the background activity in muscle and blood was generally low. Moreover, there was only low uptake of tracer in the liver and intestines. To verify the specificity of tracer binding to α5β1, a blocking study was performed in which 100 μg of unlabelled NODAGA-α5β1 ligand was injected 10 min before tracer injection (Fig. 4d–f). Uptake in α5β1-positive tumour was blocked efficiently. Prominent residual activity was present in the kidneys and bladder due to the renal excretion of the tracer. Significant nonblockable tracer uptake was also seen in the gallbladder, indicating partial elimination via the hepatobiliary pathway (Fig. 4b, e).

Time–activity curve analysis was performed by defining volumes of interest on selected organs in dynamic scans (heart, liver, kidney, muscle, and RKO and M21 tumour; Fig. 5). Apart from the rapid blood clearance and fast renal excretion of the tracer discussed above, heart, liver, kidneys and muscle showed decreasing tracer activity during the observation time, all reaching a stable washout rate 20 min after injection, as indicated by a linear decrease in the semilogarithmic plot between 20 and 90 min. RKO tumours showed stable radiotracer

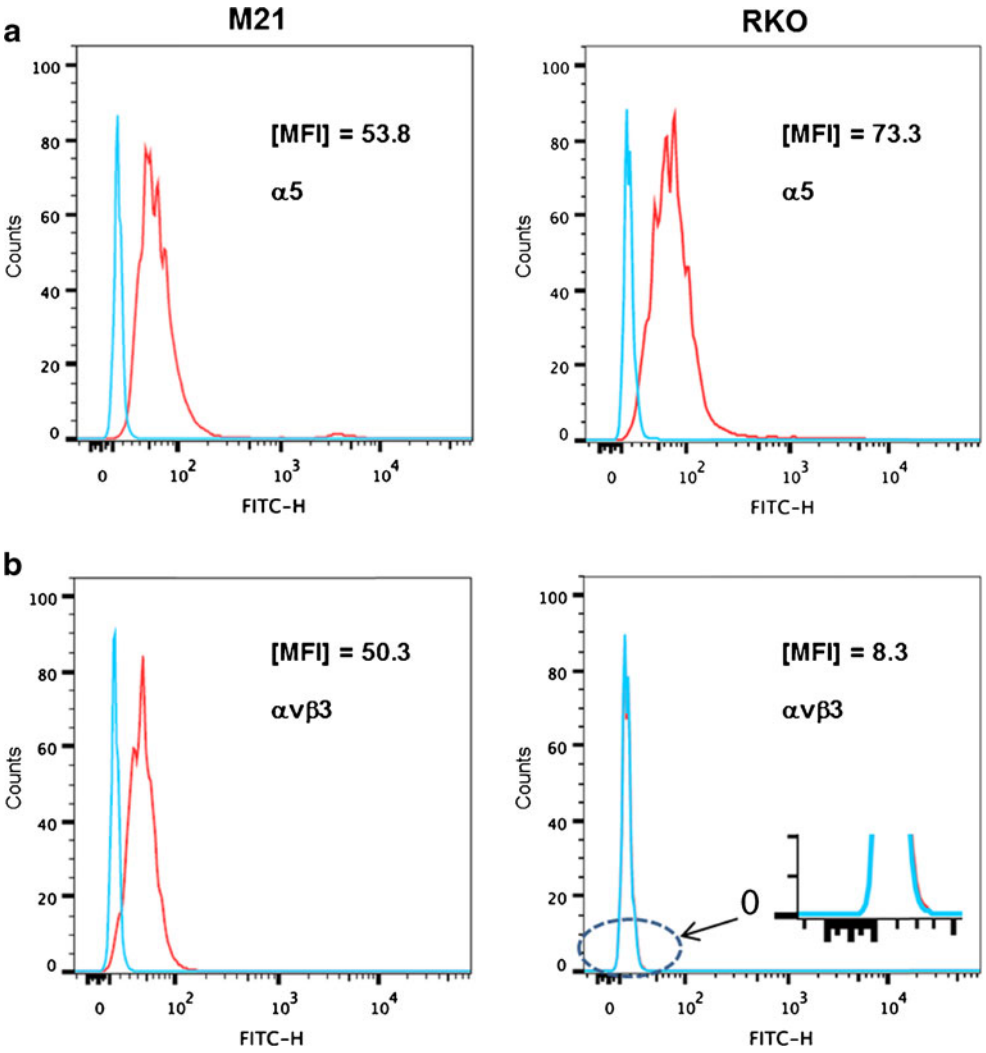

Fig. 1 FACS analysis of integrin α5β1 and αvβ3 expression on cells of the tumour cell lines M21 and RKO. The isotope control IgG (*blue line*) and specific primary antibody signal (*red line*) are shown. **a** There is a high fluorescent signal for α5β1 on the membranes of both cell lines, but higher density on RKO cells, as reflected by a mean fluorescent intensity (MFI) of 73.7 in contrast to 53.8 on M21 cells. **b** The lack of αvβ3 expression on the RKO cells in contrast to the high αvβ3 expression on the M21 cells is also apparent (MFI 8.3 vs. 50.3). For αvβ3 staining on RKO cells, the two curves are completely superimposed, confirming the absence of αvβ3 expression. *Inset* Magnification of the base of the curves reveals a red tail on the right side

activity during the 90 min scanning period, in contrast to the early high uptake in M21 tumours followed by a continuous decrease over time. Since metabolism is slower in anaesthetized mice undergoing dynamic PET

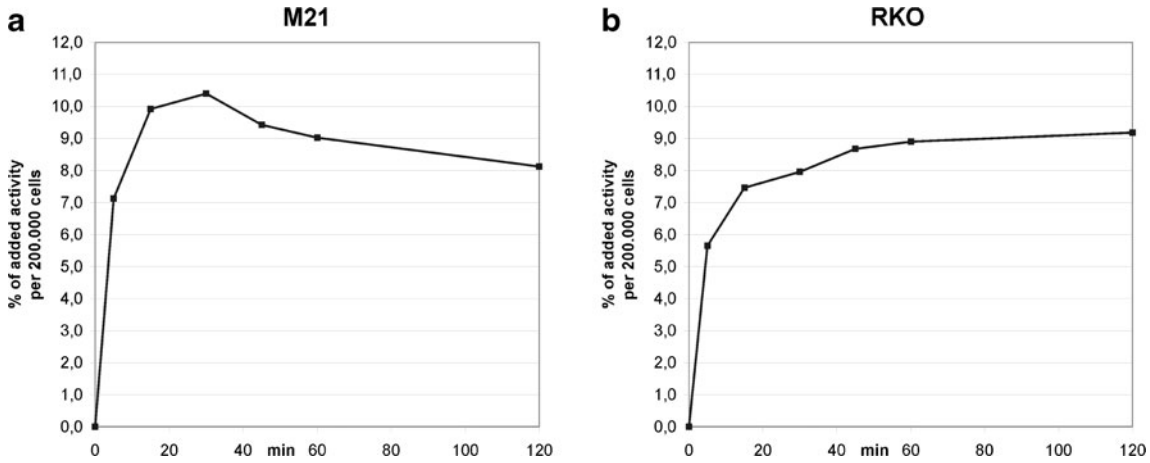

Fig. 2 Internalization assay using ^{68}Ga-labelled antagonist in M21 and RKO cells. Both cell lines were incubated with 300,000 cpm/well of ^{68}Ga-NODAGA- α5β1 over 120 min. **a**) In M21 melanoma cells, there is fast initial accumulation of radiotracer up to 30 min followed by slow release in the remaining 90 min. **b**) In contrast, in RKO cells slow early accumulation of radiotracer is followed by a stable increase in internalization in the remaining 90 min with a plateau of tracer internalization at 9.2 % of the added activity

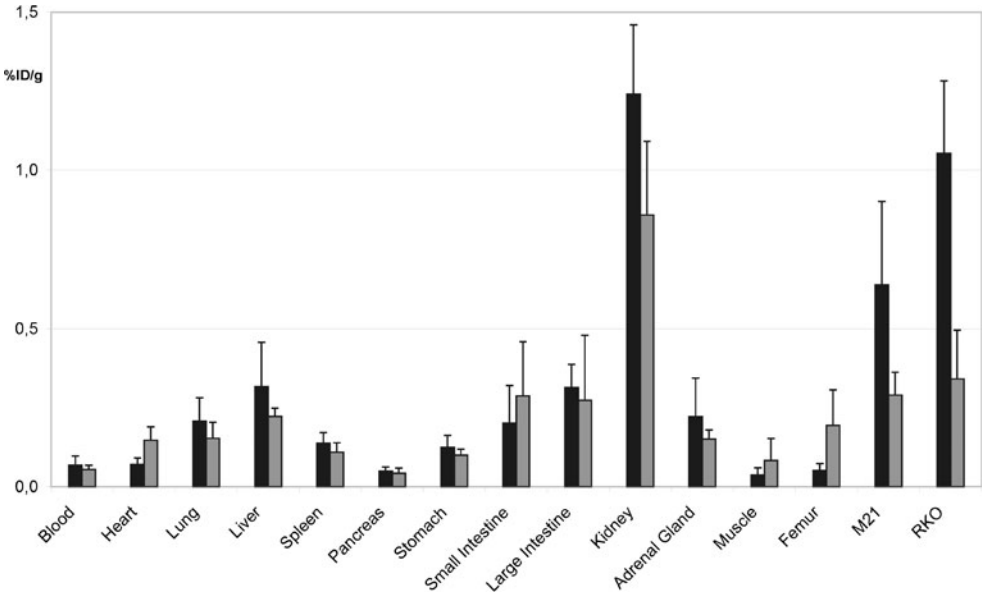

Fig. 3 Biodistribution study 90 min after injection (black bars; ten mice) and blocking experiment (grey bars; five mice). Higher tracer uptake is clearly visible in RKO tumour in comparison with M21 tumour, with a stronger reduction for RKO tumour in the blocking experiment. In accordance with the high hydrophilicity of the radiotracer (log*P*=−3.91±0.09), high uptake is seen in the kidney and low uptake in the liver

scans, final tracer accumulation in tumours and organs was somewhat higher than after static scans for which mice are anaesthetized only during tracer injection and the acquisition is from 75 to 90 min after injection. In the example shown in Fig. 5, tracer activity after 90 min was 1.84±0.25 %ID/g in RKO tumours and 1.20± 0.15 %ID/g in M21 tumours.

In vivo stability

In vivo stability was investigated in the same mouse model as used in the biodistribution and PET imaging experiments. Extraction efficiency from body fluids and tissue homogenates at 30 min after injection was 51 % for the liver, 86 % for the kidney and 79 % for tumour; binding to blood cells was 8 %. TLC analysis of urine, plasma and the filtered homogenates revealed no detectable metabolites (Fig. 6). Very high uptake was present in the urine reflecting pronounced elimination via the kidneys. These findings are in accordance with the results of biodistribution and PET imaging, indicating high in vivo stability of the ^{68}Ga-labelled antagonist.

Table 1 Tumour-to-organ ratios as calculated from the biodistribution results

Tumour	Tumour-to-organ ratio (mean±SD)	
	Blood	Muscle
RKO	17.11±5.0	29.85±9.6
M21	10.01±3.0	21.44±10.3

Discussion

We performed a detailed evaluation and characterization of the α5β1-specific antagonist FR366 coupled to the bifunctional chelator NODAGA and labelled with ^{68}Ga (^{68}Ga-NODAGA-FR366) for PET imaging of α5β1 integrin expression. The selectivity and specificity of ^{68}Ga-NODAGA-FR366 have been confirmed in previous studies [27]. The radiolabelled α5β1 ligand showed α5β1 integrin-specific uptake in vivo with good tumour/background contrast. ^{68}Ga-NODAGA-FR366 also showed high metabolic stability. Thus, this α5β1-specific PET tracer is well suited for preclinical research on the role of integrin α5β1, and is a potential candidate for translation to first studies in humans.

Since the initial observation that integrin αvβ3 is upregulated on the vasculature of certain tumours, several inhibitors for this integrin and the closely related integrin αvβ5 have been tested for their antiangiogenic activity [30, 31]. Monoclonal antibodies, such as LM609, and various low molecular weight molecules based on the tripeptide RGD have been shown to block angiogenesis in response to growth factors in tumours and in retinal angiogenesis [32–34]. These results led to the idea that these two integrins have proangiogenic activity. However, studies on genetically altered mice have shown that animals lacking β3 are viable and fertile, as are mice lacking β5 [35]. Furthermore, mice lacking αv also show extensive angiogenesis [36]. Therefore, there is a discrepancy between the genetic results and those obtained using blocking agents, antibodies and low molecular weight reagents targeting those integrins. In contrast, genetic ablation of β1 is lethal to the embryo, causing major vascular defects α5β1 and its natural ligand fibronectin are lacking [37, 38]. Extensive research has been carried out to develop

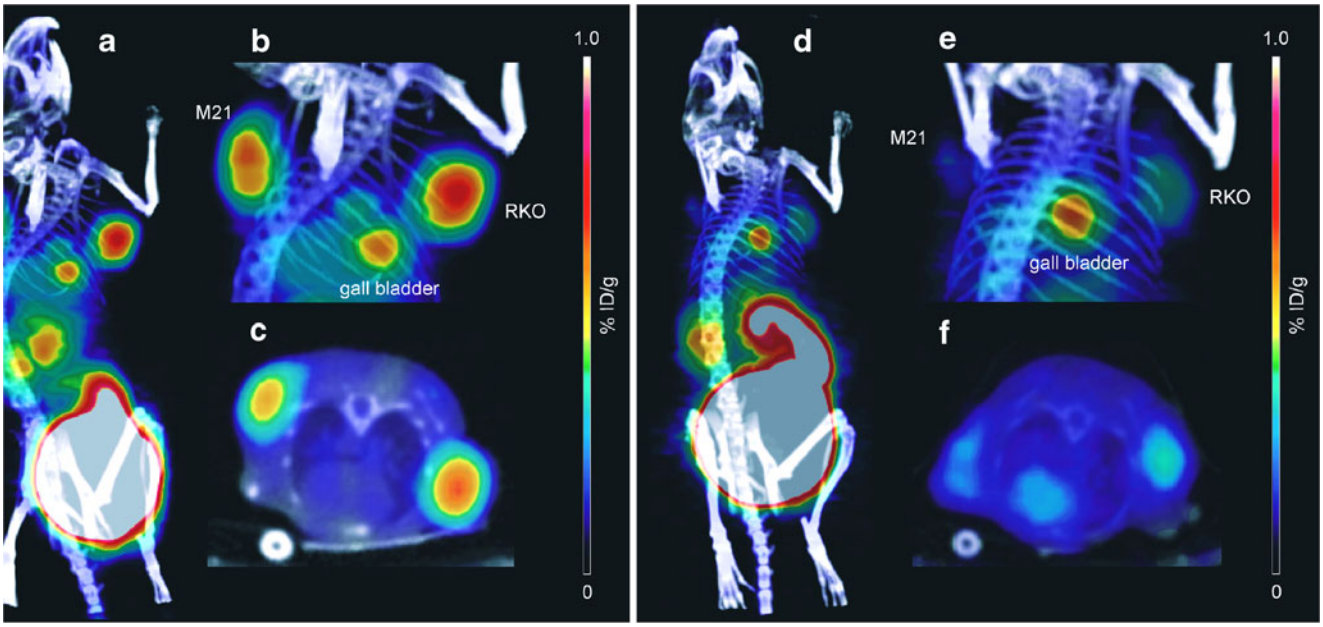

Fig. 4 MicroPET maximum intensity projection scans of mice bearing M21 and RKO tumour xenografts in the left and right shoulders acquired 75 – 90 min after injection. **a–c** Uptake of ^{68}Ga-labelled α5β1 antagonist. **d**. **e** Blocking experiment (injection of 100 μg unlabelled ligand 10 min before radiotracer injection). **a**. **d** Whole-body PET/CT fusion images. **c**. **f** Axial projections showing the tumours in both shoulders: tracer uptake is higher in the RKO tumour (right shoulder) than in the M21 tumour (left shoulder)

peptidomimetic integrin ligands based on the tripeptide RGD, which is recognized by the two integrins αvβ3 and αvβ5 [5]. Peptidomimetic substances of this kind have already been synthesized and tested for selectivity [27]. Thus, our novel compound provides a valuable tool for further elucidation of the role of integrin α5β1 in vivo. Furthermore, based on the data discussed above, imaging of α5β1 expression might be even better as a biomarker of angiogenesis and tumour behaviour than imaging of integrin αvβ3.

We chose the strategy of radiolabelling using NODAGA as a chelator, as in previous studies with αvβ3-specific ^{68}Ga-DOTA-based radiotracers, relatively high amounts of protein-bound activity were found that resulted in pronounced background activity especially in the blood, which is unfavourable for in vivo imaging. This is related to the fact that the $^{68}Ga^{3+}$ ion is too small to optimally fit in the DOTA cage, and hence $^{68}Ga^{3+}$ is released slowly [39]. The triazacyclononane cage of NODAGA ligand shows better

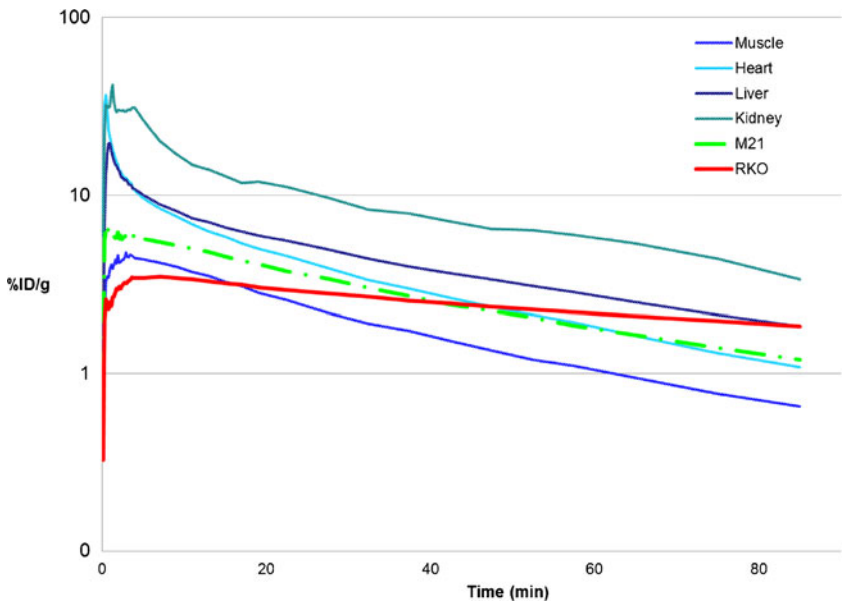

Fig. 5 Representative time–activity curves for RKO and M21 tumours from a 90-min dynamic PET scan in a mouse injected with ^{68}Ga-NODAGA-FR366 antagonist. RKO tumour shows stable retention of activity (*red line*) while M21 tumour shows a steady decrease in activity (*green line*)

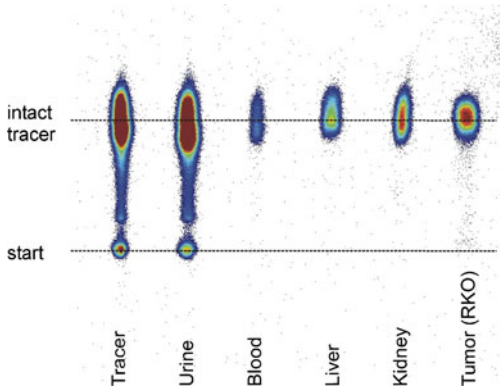

Fig. 6 TLC analysis of urine, plasma and tissue extracts from a mouse bearing a RKO tumour xenograft that received 30 – 40 MBq of ^{68}Ga-labelled FR366 antagonist and was killed 30 min after injection

complexation properties for metal ions with radii similar to that of Ga^{3+} than the commonly used DOTA. Functionalization of the α5β1-specific antagonist with NODAGA did not alter its high affinity, as has been shown previously in integrin binding assays. The antagonist provided an affinity for α5β1 of 2.3±0.02 nM and the NODAGA-coupled ligand 1.3±0.08 nM [27]. ^{68}Ga-labelling of the precursor was performed in an automated fashion with good reproducibility and resulted in a radiolabelled product with high specific activity and radiochemical purity, which allowed its use without further purification for in vitro and in vivo experiments. Thus clinical translation with efficient radiolabelling should be feasible with our compound [29].

The human colon carcinoma cell line RKO and the human melanoma cell line M21 were chosen for this study. Both cell lines express α5β1 integrin with different intensities and M21 additionally shows high expression of αvβ3 while this integrin subtype is almost absent on RKO cells as demonstrated by FACS analysis. These results strongly support the specificity and selectivity of the α5β1 antagonist, as previously reported [27]. In vitro internalization studies showed uptake of the tracer in both cell lines with different binding kinetics. In M21 cells, the tracer was washed out slowly after fast initial incorporation in the first 30 min. In RKO cells, tracer uptake was also rapid in the first 30 min of incubation, but then showed a steady increase during the whole 120-min incubation period.

A possible explanation for the different kinetics of tracer incorporation could be the differential regulation of α5β1 integrin recycling/endocytosis or membrane expression modulation due to cytoplasmic effector molecules interacting with β1 integrin (i.e. guanine nucleotide exchange factor Brag2, Rho kinase signalling, caveolin-1) [40–42]. Molecular biological studies using M21 and RKO tumour cells are necessary to verify our hypothesis, and to elucidate which cytoplasmic effector is involved in the differential regulation of α5β1 integrin membrane expression and how the effector is involved, and to elucidate how these biomolecular modulations are correlated with the differences in tracer internalization. In biodistribution experiments and PET/CT imaging performed in mice xenografted with both cell lines, we found a difference in tracer uptake with higher accumulation in RKO tumour than in M21 tumour.

The difference in in vivo tumour tracer uptake could also be explained by different α5β1 integrin recycling/endocytosis or membrane expression modulation, which in turn may be responsible of differences in tumour vascularization [40–42]. In PET/CT images in mice, higher accumulation of ^{68}Ga-NODAGA-FR366 in the gallbladder than in other main organs was visible. The transfer of activity from the liver into the gallbladder and into the small intestine is a dynamic and stepwise process, and PET images reflect only one particular moment in that process. that is the phase when most of the activity in the liver has already been transferred into the gallbladder shortly before its release into the small intestine. Specificity of binding was confirmed by a strong reduction in tracer accumulation in mice previously injected with an excess of unlabelled antagonist in both xenografted tumours. High in vivo stability of the radiotracer was proved by metabolic studies, with radioactivity found in the urine as result of kidney excretion.

Currently, to our knowledge, only one other study on α5β1 in vivo PET imaging is available. This study investigated the use of a disulphide bridged cyclic peptide, but in vivo biokinetic evaluation is missing [43]. The use of small-animal MRI for imaging α5β1 in vivo has also been reported [44]. While MRI provides excellent soft-tissue contrast and good spatial resolution, the relatively large concentrations of imaging probes necessary due to the limited sensitivity is a disadvantage compared with PET/CT. Even more important, due to the higher doses of imaging probes necessary, clinical translation is challenging, in contrast to radiotracers of which only minimal amounts need be injected. In addition, the high resolution and sensitivity of PET/CT might allow the correlation of in vivo tracer uptake and the expression of integrin α5β1 in patient specimens using immunohistochemistry.

Conclusion

In this study, we performed the first detailed biokinetic and metabolic study of the α5β1-specific antagonist FR366 coupled to the chelator NODAGA and labelled with ^{68}Ga for imaging α5β1 expression in vivo in animal tumour models. The radiolabelled α5β1 ligand showed high affinity for integrin α5β1, both in vitro and in vivo, specific integrin α5β1 uptake in vivo, and good imaging properties in small-animal PET/CT studies with good tumour-to-background contrast and metabolic stability. Thus, this tracer is a promising compound not only for diagnostic imaging and disease

monitoring but also for therapeutic interventions involving the selective targeting of specific integrins.

Acknowledgments We thank Christina Lesti, Rosel Oos and Marianna Kallinger for technical assistance (cell culture and animal handling), Martina Anton and Edelburga Hammerschmid for help with the FACS analysis and Sybille Reder, Markus Mittelhäuser and Marco Lehmann for performing the animal PET/CT experiments.

Author contributions C.D. optimized the FACS analysis protocol and measurements, elaborated and prepared the PET/CT images, performed the data analysis, and wrote the manuscript. K.P. carried out ^{68}Ga-labelling, performed cell binding studies, the FACS analysis and in vivo experiments (biodistribution, metabolic stability, PET/CT analysis). S.N. and F.R. synthesized and characterized the integrin antagonist. J.N. and H.J.W. proof-read the manuscript and provided advice on ^{68}Ga labelling. A.J.B. and M.S. were responsible for the molecular imaging experiments. A.J.B., M.S. and H.K. initiated and supervised the project. All authors contributed to writing and editing the manuscript.

Compliance with ethical standards

Funding This work was carried out within the MOBITUM project P3 "Improved ligands for quantitative monitoring of integrin expression" (MOBITEC/MOBITUM 01EZ0826) at TU Munich and was supported partially by ERC grant MUMI, ERC-2011-ADG_20110310, by the SFB 824 project C5 "Evaluation of imaging of αVβ3 expression with PET for response assessment of antiangiogenic therapies" and the Center of Integrated Protein Science Munich (CIPSM). H.K. is grateful for financial support from the Center of Integrated Protein Science Munich (CIPSM) and from King Abdulaziz University KAU (grant no. HiCi/25-3-1432).

Conflicts of interest None.

Ethical approval for animal studies All animal experiments were approved by the "Regierung von Oberbayern" (animal permission no. 55.2-1-45-2531-94-10) and were performed in accordance with current animal welfare regulations in Germany.

References

1. Desgrosellier JS, Cheresh DA. Integrins in cancer: biological implications and therapeutic opportunities. Nat Rev Cancer. 2010;10(1):9–22.
2. Harburger DS, Calderwood DA. Integrin signalling at a glance. J Cell Sci. 2009;122(Pt 2):159–63.
3. Hynes RO. Integrins: bidirectional, allosteric signaling machines. Cell. 2002;110:673–87.
4. Shattil SJ, Kim C, Ginsberg MH. The final steps of integrin activation: the end game. Nat Rev Mol Cell Biol. 2010;11(4):288–300.
5. Thumshirn G, Hersel U, Goodman SL, Kessler H. Multimeric cyclic RGD peptides as potential tools for tumor targeting: solid-phase peptide synthesis and chemoselective oxime ligation. Chemistry. 2003;9(12):2717–25.
6. Meyer A, Auernheimer J, Modlinger A, Kessler H. Targeting RGD recognizing integrins: drug development, biomaterial research, tumor imaging and targeting. Curr Pharm Des. 2006;12:2723–47.
7. Schottelius M, Laufer B, Kessler H, Wester HJ. Ligands for mapping alphavbeta3-integrin expression in vivo. Acc Chem Res. 2009;42(7):969–80.
8. Goodman SL, Picard M. Integrins as therapeutic targets. Trends Pharmacol Sci. 2012;33(7):405–12.
9. Aumailley M, Gurrath M, Müller G, Calvete J, Timpl R, Kessler H. Arg-Gly-Asp constrained within cyclic pentapeptides. Strong and selective inhibitors of cell adhesion to vitronectin and laminin fragment P1. FEBS Lett. 1991;291(1):50–4.
10. Dechantsreiter MA, Planker E, Mathä B, Lohof E, Hölzemann G, Jonczyk A, et al. N-Methylated cyclic RGD peptides as highly active and selective alpha(V)beta(3) integrin antagonists. J Med Chem. 1999;42(16):3033–40.
11. Mas-Moruno C, Rechenmacher F, Kessler H. Cilengitide: the first anti-angiogenic small molecule drug candidate design, synthesis and clinical evaluation. Anticancer Agents Med Chem. 2010;10(10):753–68.
12. Haubner R, Wester H-J, Burkhart F, Senekowitsch-Schmidtke R, Weber W, Goodman SL, et al. Glycosylated RGD-containing peptides: tracer for tumor targeting and angiogenesis imaging with improved biokinetics. J Nucl Med. 2001;42(2):326–36.
13. Gruner SA, Locardi E, Lohof E, Kessler H. Carbohydrate-based mimetics in drug design: sugar amino acids and carbohydrate scaffolds. Chem Rev. 2002;102(2):491–514.
14. Haubner R, Bruchertseifer F, Bock M, Kessler H, Schwaiger M, Wester HJ. Synthesis and biological evaluation of a (99m)Tc-labeled cyclic RGD peptide for imaging the alphavbeta3 expression. Nuklearmedizin. 2004;43(1):26–32.
15. Haubner R, Kuhnast B, Mang C, Weber WA, Kessler H, Wester HJ, et al. [18F]Galacto-RGD: synthesis, radiolabeling, metabolic stability, and radiation dose estimates. Bioconjug Chem. 2004;15(1):61–9.
16. Haubner R, Weber WA, Beer AJ, Vabuliene E, Reim D, Sarbia M, et al. Noninvasive visualization of the activated alphavbeta3 integrin in cancer patients by positron emission tomography and [18F]Galacto-RGD. PLoS Med. 2005;2(3):e70.
17. Beer AJ, Haubner R, Goebel M, Luderschmidt S, Spilker ME, Wester HJ, et al. Biodistribution and pharmacokinetics of the alphavbeta3-selective tracer 18F-galacto-RGD in cancer patients. J Nucl Med. 2005;46(8):1333–41.
18. Beer AJ, Haubner R, Sarbia M, Goebel M, Luderschmidt S, Grosu AL, et al. Positron emission tomography using [18F]Galacto-RGD identifies the level of integrin alpha(v)beta3 expression in man. Clin Cancer Res. 2006;12(13):3942–9.
19. Garmy-Susini B, Varner JA. Integrins in angiogenesis and lymphangiogenesis. Nat Rev Cancer. 2008;8(8):604–17.
20. Robinson SD, Hodivala-Dilke KM. The role of β3-integrins in tumor angiogenesis: context is everything. Curr Opin Cell Biol. 2011;23(5):630–7.
21. Kim S, Bell K, Mousa SA, Varner JA. Regulation of angiogenesis in vivo by ligation of integrin alpha5beta1 with the central cell-binding domain of fibronectin. Am J Pathol. 2000;156(4):1345–62.
22. Barkan D, Kleinman H, Simmons JL, Asmussen H, Kamaraju AK, et al. Inhibition of metastatic outgrowth from single dormant tumor cells by targeting the cytoskeleton. Cancer Res. 2008;68(15):6241–50.
23. Kato H, Liao Z, Mitsios JV, Wang HY, Deryugina EI, Varner JA, et al. The primacy of β1 integrin activation in the metastatic cascade. PLoS One. 2012;7(10):e46576.
24. Park CC, Zhang HJ, Yao ES, Park CJ, Bissell MJ. Beta1 integrin inhibition dramatically enhances radiotherapy efficacy in human breast cancer xenografts. Cancer Res. 2008;68(11):4398–405.
25. Janouskova H, Maglott A, Leger DY, Bossert C, Noulet F, Guerin E, et al. Integrin α5β1 plays a critical role in resistance to temozolomide by interfering with the p53 pathway in high-grade glioma. Cancer Res. 2012;72(14):3463–70.
26. Rechenmacher F, Neubauer S, Polleux J, Mas-Moruno C, De Simone M, Cavalcanti-Adam EA, et al. Functionalizing αvβ3- or α5β1-selective integrin antagonists for surface coating: A method

to discriminate integrin subtypes in vitro. Angew Chem Int Ed Engl. 2013;52(5):1572–5.
27. Neubauer S, Rechenmacher F, Beer AJ, Curnis F, Pohle K, D'Alessandria C, et al. Selective imaging of the angiogenic relevant integrins αvβ3 and α5β1. Angew Chem Int Ed Engl. 2013;52(44): 11656–9.
28. Neubauer S, Rechenmacher F, Brimioulle R, Di Leva FS, Bochen A, Sobahi TR, et al. Pharmacophoric modifications lead to superpotent αvβ3 integrin ligands with suppressed α5β1 activity. J Med Chem. 2014;57(8):3410–7.
29. Pohle K, Notni J, Bussemer J, Kessler H, Schwaiger M, Beer AJ. 68Ga-NODAGA-RGD is a suitable substitute for 18F-Galacto-RGD and can be produced with high specific activity in a cGMP/GRP compliant automated process. Nucl Med Biol. 2012;39(6): 777–84.
30. Hodivala-Dilke K. alphavbeta3 integrin and angiogenesis: a moody integrin in a changing environment. Curr Opin Cell Biol. 2008;20(5):514–9.
31. Heckmann D, Meyer A, Laufer B, Zahn G, Stragies R, Kessler H. Rational design of highly active and selective ligands for the α5β1 integrin receptor. Chembiochem. 2008;9(9):1397–407.
32. Friedlander M, Brooks PC, Shaffer RW, Kincaid CM, Varner JA, Cheresh DA. Definition of two angiogenic pathways by distinct alpha v integrins. Science. 1995;270(5241):1500–2.
33. Friedlander M, Theesfeld CL, Sugita M, Fruttiger M, Thomas MA, Chang S, et al. Involvement of integrins alpha v beta 3 and alpha v beta 5 in ocular neovascular diseases. Proc Natl Acad Sci U S A. 1996;93(18):9764–9.
34. Hodivala-Dilke KM, McHugh KP, Tsakiris DA, Rayburn H, Crowley D, Ullman-Culleré M, et al. Beta3-integrin-deficient mice are a model for Glanzmann thrombasthenia showing placental defects and reduced survival. J Clin Invest. 1999;103(2):229–38.
35. Reynolds LE, Wyder L, Lively JC, Taverna D, Robinson SD, Huang X, et al. Enhanced pathological angiogenesis in mice lacking beta3 integrin or beta3 and beta5 integrins. Nat Med. 2002;8(1):27–34.
36. Bader BL, Rayburn H, Crowley D, Hynes RO. Extensive vasculogenesis, angiogenesis, and organogenesis precede lethality in mice lacking all alpha v integrins. Cell. 1998;95(4):507–19.
37. George EL, Georges-Labouesse EN, Patel-King RS, Rayburn H, Hynes RO. Defects in mesoderm, neural tube and vascular development in mouse embryos lacking fibronectin. Development. 1993;119(4):1079–91.
38. Fässler R, Meyer M. Consequences of lack of beta 1 integrin gene expression in mice. Genes Dev. 1995;9(15):1896–908.
39. Decristoforo C, Hernandez Gonzalez I, Carlsen J, Rupprich M, Huisman M, Virgolini I, et al. 68Ga- and 111In-labeled DOTA-RGD peptides for imaging of alpha v beta 3 integrin expression. Eur J Nucl Med Mol Imaging. 2008;35(8):1507–15.
40. White DP, Caswell PT, Norman JC. alpha v beta3 and alpha5beta1 integrin recycling pathways dictate downstream Rho kinase signaling to regulate persistent cell migration. J Cell Biol. 2007;177(3): 515–25.
41. Shi F, Sottile J. Caveolin-1-dependent beta1 integrin endocytosis is a critical regulator of fibronectin turnover. J Cell Sci. 2008;121(Pt 14):2360–71.
42. Manavski Y, Carmona G, Bennewitz K, Tang Z, Zhang F, Sakurai A, et al. Brag2 differentially regulates β1- and β3-integrin-dependent adhesion in endothelial cells and is involved in developmental and pathological angiogenesis. Basic Res Cardiol. 2014;109(2):404.
43. Haubner R, Maschauer S, Einsiedel J, Eder IE, Rangger C, Gmeiner P, et al. H-CRRETAWAC-OH, a lead structure for the development of radiotracer targeting integrin α5β1? Biomed Res Int. 2014;2014:243185. doi:10.1155/2014/243185.
44. Schmieder AH, Caruthers SD, Zhang H, Williams TA, Robertson JD, Wickline SA, et al. Three-dimensional MR mapping of angiogenesis with alpha5beta1(alpha nu beta3)-targeted theranostic nanoparticles in the MDA-MB-435 xenograft mouse model. FASEB J. 2008;22(12):4179–89.